ISBN: 978-3-95450-206-6 doi:10.18429/JACoW-FLS2018-WEP2PT008

MICROBUNCHING INSTABILITY STUDY IN THE LINAC-DRIVEN FERMI FEL SPREADER BEAM LINE*

S. Di Mitri †, S. Spampinati, Elettra – Sincrotrone Trieste S. C. p. A., Basovizza, Trieste, Italy

Abstract

Suppression of microbunching instability (MBI) along high brightness electron beam delivery systems is a priority for Free Electron lasers (FELs) aiming at very narrow bandwidth. The impact of MBI on FEL spectral brilliance is aggravated by the growing demand for multi-user FEL facilities, which adopt multi-bend switchyard lines traversed by high charge density electron beams. This study provides practical guidelines to switchyards design largely immune to MBI, by focusing on the FERMI FEL Spreader line. First, two MBI analytical models [Z. Huang and K.-J- Kim, Phys. Rev. Special Topics - Accel. Beams 5, 074401 (2002); R.A. Bosch, K.J. Kleman and J. Wu, Phys. Rev. Special Topics - Accel. Beams 11, 090702 (2008)] are successfully benchmarked along the accelerator. Being the second model flexible enough to describe an arbitrary multi-bend line, and found it in agreement with particle tracking and experimental results, it was used to demonstrate that a newly proposed Spreader optics provides unitary MBI gain while preserving the electron beam brightness.

INTRODUCTION

In FEL facilities with multiple undulator lines, the strength of the microbunching instability (MBI) is reinforced in multi-bend switchyard lines that connect the accelerator to the individual undulator lines [1–5]. Due to the presence of several dipole magnets traversed by a high charge density beam, those switchyards can dramatically amplify residual density and energy modulations present on the electron beam at the exit of the linac. This study examines MBI growth in the accelerator and switchyard, and provides practical guidelines for switchyard optics designs that are largely immune to MBI, i.e., with unity gain of the instability. We provide a specific solution for the FERMI FEL [6,7] spreader beam line that can be easily implemented within the current space and with existing magnets [8].

MBI in the FERMI linac has been continuously studied since the early stages of machine design [9–11]. MBI concerns led to the choice of operating FERMI both with a so-called laser heater (LH) [12,13], a tool that suppresses MBI via energy Landau damping, and in general using only one active magnetic bunch length compressor [9]. The FERMI laser heater usually improves the FEL spectral brilliance by up to factors 3 or more [13,14]. Nonetheless, there is experimental evidence [11,15] of both enlargement and shot-to-shot variability of the spectral bandwidth for wavelengths 10 nm or shorter. Provisionally, this degradation is assigned to effects originating with residual MBI from the linac and to its further amplification in the spreader.

This paper aims to elucidate the role of the FERMI spreader on the MBI development.

MODELS

The reader is sent to [16] the MBI model developed by Z. Huang and K.-J. Kim (henceforth labeled the "HK-model"), and based on integral equations for the bunching factor, i.e., the Fourier transform of the bunch current density function. The reader is sent to [17] for the MBI model developed by R. Bosch et al. (henceforth labeled the "B-model"), and based on matrix formalism. All collective effects are described by frequency-dependent effective impedances separately calculated for linac straight sections and chicane dipole bend sections.

The HK- and the B-models have been compared by adopting a shot-noise driven initial density modulation that has no corresponding energy modulation. The initial bunching factor is taken to be:

$$b_{sn}(\lambda_0) = \sqrt{\frac{2ec}{I_0\lambda_0}} \tag{1}$$

An additional indicator of the MBI strength, used for the comparison of the two models, is given by the amount of energy spread accumulated by the end of the beam line. Assuming that the final energy modulations are entirely converted into uncorrelated energy spread, the equivalent uncorrelated energy spread (RMS value) from the MBI growth is calculated as the integral of the final energy modulation over all (or user-specified) frequency components [18]:

$$\sigma_{E,MBI} = \frac{1}{2\pi\sqrt{2}}\sqrt{\int d\lambda \frac{\Delta E^2_{MBI}(\lambda)}{\lambda}} \tag{2}$$

The HK- and the B-model both include originally Coherent Synchrotron Radiation (CSR) and Longitudinal Space Charge (LSC) impedance, energy- and transverse emittance-induced Landau damping. They were further revised for the purpose of comparison as follows:

i) the LSC impedance is averaged over the transverse beam dimensions, which vary along the linac, according to the prescriptions in [19,20];
ii) the MBI gain is evaluated by keeping the initial bunching factor, i.e., the low gain regime is retained together with the high gain contribution [13];
iii) the effect of the LH on the electron beam initial energy distribution was calculated as in [21], assuming a laser pulse whose transverse waist size is matched at the midpoint of the LH undulator to that of the electron beam;
iv) for a fair comparison of the two models, the B-model was applied to the FERMI linac by excluding the im-

ISBN: 978-3-95450-206-6 doi:10.18429/JACoW-FLS2018-WEP2PT008

pedance contributions of Coherent Edge Radiation (CER), LSC in the BC1 drift sections, and the geometric longitudinal impedance of RF structures.

CODES BENCHMARKING

The FERMI linac-plus-spreader beam line is sketched in Fig.1. The linac is composed of multiple accelerating structures interleaved by two magnetic bunch compressors (BC1, BC2). BC1 only is active during standard FEL operation. Each branch of the spreader is a dog-leg made of two modified double bend achromatic cells (MDBAs), separated by quadrupole magnets [22]. Since the impact of MBI on the FEL spectrum is stronger at shorter FEL wavelengths, only that part of the spreader that feeds the FEL-2 branch line is considered in the following calculations and discussion.

Figures 2 and 3 compare the two models' prediction, with and without LH. Table 1 compares the final uncorrelated energy spread as computed by the quadratic sum of the initial one and that one induced by MBI (see Eq.2), for the two LH scenarios illustrated in Figs. 2 and 3.

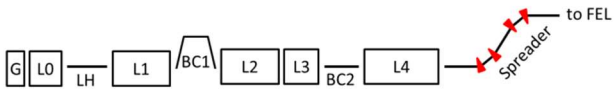

Figure 1: Sketch, not to scale, of the FERMI linac-plus-spreader FEL-2 beam line. This study applies from the exit of L0 to the spreader end. Only the first magnetic bunch compressor, BC1, is active and for these calculations is presumed to give perfect linear compression. Copyright of APS (2018).

Table 1: Total uncorrelated energy spread (RMS value) at the end of the FERMI linac (see Figs.2,3). The energy modulation induced by MBI over the initial wavelength range 0.5–200 μm is assumed to convert entirely into uncorrelated energy spread (see Eq.2).

Laser Heater	HK-model	B-model	Unit
Off	331	338	keV
10 keV	102	110	keV

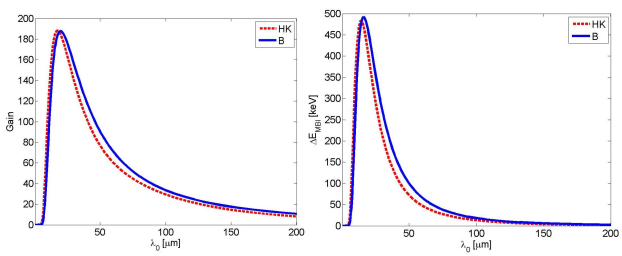

Figure 2: Comparison of MBI gain (top) and energy modulation amplitude (bottom) at the end of the FERMI linac vs. the *initial* density modulation wavelength. The two curves correspond to the separate predictions by the HK-model [16] (dashed line) and the B-model [17] (solid line). The laser heater is off. Copyright of APS (2018).

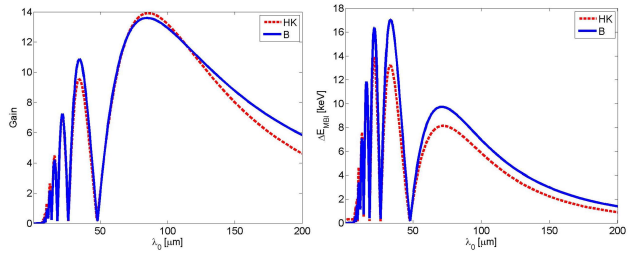

Figure 3: Comparison of MBI gain (top) and energy modulation amplitude (bottom) at the end of the FERMI linac vs. the *initial* density modulation wavelength. The two curves correspond to the separate predictions by the HK-model [16] (dashed line) and the B-model [17] (solid line). The laser heater is off. Copyright of APS (2018).

MBI IN THE FERMI LINAC + SPREADER

The development of MBI along the *whole* FERMI beam delivery system, now including RF impedances and CER, is illustrated in Fig.4. The LH intensity is set to the nominal 10 keV RMS energy spread level. By the end of the FERMI spreader, the total MBI gain increases by a factor up to 10 relative to that seen at the end of the linac, and the energy modulation amplitudes have more than doubled at shorter wavelengths. The up to 40 keV energy modulation amplitudes accumulated at the spreader exit approach the level of the natural beam energy spread in the absence of instability. Moreover, the MBI modulations lie in the *final* wavelength range 0.5–5 μm. These wavelengths are shorter than the FERMI external seed laser pulse length (approximately 30 μm long), and generally longer than the FEL-2 cooperation length (this is 0.3–0.8 μm for FEL output wavelengths in the range 4–10 nm). Thus, one could expect a serious impact of such modulations on the FEL spectrum in terms of shot-to-shot spectral variability and generalized bandwidth enlargement, due to excitation of sidebands on the main seeded line [11,23,24]. These considerations fully justify serious efforts to reducing the contribution of the spreader to the global MBI dynamics, as is done in the next Section.

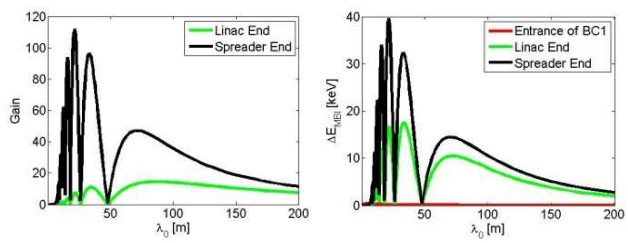

Figure 4: Gain (left) and energy modulation amplitude at the end of the FERMI linac (green) and of the linac-plus-spreader beam line (black). The laser heater is set at 10 keV RMS energy spread before compression. Copyright of APS (2018).

NEW SPREADER OPTICS

The study reported in [25,26] suggests that a quasi-isochronous and achromatic spreader line would see a much reduced MBI gain. More recently, the simultaneous requirement of small MBI gain and preservation of the

ISBN: 978-3-95450-206-6 doi:10.18429/JACoW-FLS2018-WEP2PT008

transverse beam emittance in the presence of CSR head-tail instability [27] led to the prescription of a locally-isochronous beam line whose properties include small variations of R_{56}, π-betatron phase advance between consecutive dipole magnets, low betatron function and relatively large alpha-function at the dipoles [28] (all terms correspond to the bending plane).

These prescriptions were incorporated into a new FERMI FEL-2 spreader design, where the physical length, position and bending angles of the actual beam line were retained. The total R_{56} of the beam line is reduced from its present value of 680 μm down to 1 μm by virtue of the reversed sign of the dispersion function inside the two inner dipoles of the spreader branch.

A comparison of the present (or standard) and new linear optics functions, as well as of the R_{56} term along the line, is given in Fig.5. Figure 6 replicates Fig.4 for the new optics. The new spreader design is substantially transparent to any incoming modulation induced by MBI in the linac, since the curves at the linac end (green) and at the spreader end (black) tend to superimpose, as a consequence of a unity gain through the beam line. It is worth pointing out that the new design requires only a re-adjustment of the strengths of the quadrupole magnets internal to the MDBAs that lies within a range fully compatible with the FERMI operation up to 1.5 GeV beam energy. The present spreader optics preserves the beam horizontal normalized emittance from the CSR head-tail instability at 0.1 μm level [22].

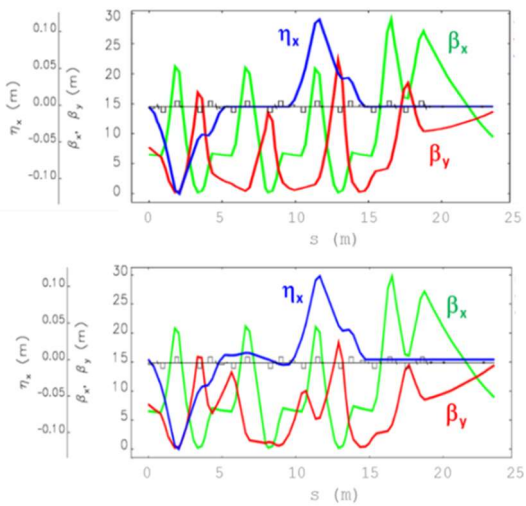

Figure 5: Linear optics functions along the FERMI spreader for the *present* (top) and new optics design. Copyright of APS (2018).

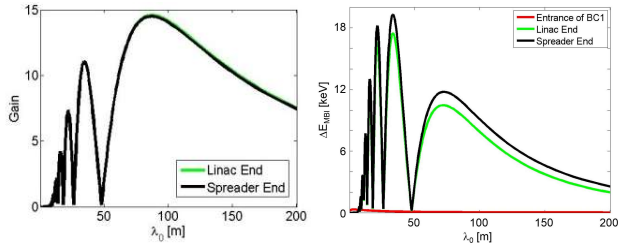

Figure 6: Gain (left) and energy modulation amplitude at the end of the FERMI linac (green) and linac-plus-spreader beam line (black), for the new spreader optics. The laser heater is set at 10 keV RMS energy spread before compression. Copyright of APS (2018).

EXPERIMENTAL RESULTS

The intensity of optical transition radiation (OTR) emitted by the electron beam passing through a 100 μm thick-Al foil (OTR screen) at the end of the FERMI spreader was used as an indicator of the MBI gain at optical wavelengths (the CCD of the OTR screen system is sensitive to radiation wavelengths < 3 μm), as coherent density modulations should strongly increase the OTR emission. The inset of Figure 7 shows the reduction of the bunching factor predicted by the B-model when the new spreader optics is adopted (solid line), in comparison to the standard optics (dashed line). The main plot shows the measured OTR signal integrated over the physical region occupied by the beam spot at the screen, and averaged over many shots. The OTR signal is shown as a function of the LH pulse energy, for the standard (dashed line) and the new spreader optics (solid line). Control of beam sizes was accomplished by means of the last 4 quadrupoles of the spreader line, installed upstream the screen and in a dispersion-free region. In accordance with the model, higher pulse energies suppress the instability at longer wavelengths [13].

The OTR intensity in the presence of the standard spreader optics shows a large sensitivity to the LH setting. A coherent OTR emission shows up as large signal intensity for low heating level, and it disappears for LH energies higher than 1 μJ. On the contrary, the OTR intensity collected in the presence of the new Spreader optics is largely insensitive to the LH setting. The OTR signal value stays at the level of that one collected with the standard optics and large LH energy, ~4 μJ.

In order to verify the simultaneous suppression of MBI and preservation of the beam transverse emittance, the emittances were measured with the quadrupole scan technique [29] at the end of the spreader. The new spreader optics, as well as the standard one, preserves the horizontal emittance from CSR head-tail instability.

ISBN: 978-3-95450-206-6 doi:10.18429/JACoW-FLS2018-WEP2PT008

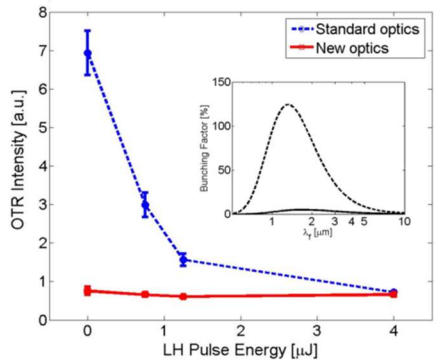

Figure 7: OTR intensity measured at the end of the FERMI spreader vs. LH pulse energy, for the standard (blue dashed) and the new optics configuration (red solid). Error bars are the RMS fluctuation of the OTR signal over 500 consecutive shots. In the inset: bunching factor calculated at the end of the linac-plus-spreader beam line with LH off vs. final (compressed) wavelength of modulation, for the spreader standard (dashed) and new optics (solid). Copyright of APS (2018).

CONCLUSION

A systematic comparison of two analytical models [16,17] for MBI growth in the FERMI linac has been done, including transversally-averaged LSC impedance and realistic LH effect. The two codes are found in good quantitative agreement. Given the flexibility of the B-model introduced in [17] for describing the MBI in an arbitrary transfer line, we applied it to the actual FERMI spreader beam line to FEL-2, where the code was additionally benchmarked with particle tracking runs. This study revealed a significant contribution of the spreader to the amplification of residual MBI exiting the linac, even in the situation where the FERMI laser heater is run at its nominal intensity. As a result, coherent energy modulations at the level of tens of keV in the final wavelength range 0.5–5 μm are expected at the undulator entrance. Due to sideband formation, these modulations are expected to degrade the FEL spectral brilliance at output radiation wavelengths shorter than ~10 nm.

A new spreader optics was designed to simultaneously minimize the spreader MBI gain and preserve the horizontal beam emittance from growth associated with the CSR head-tail instability. Importantly, the new solution does not require any physical change in the existing layout and could be readily implemented. Experimental tests of the new spreader optics confirmed both the negligible MBI gain as measured by the OTR signal, and the preserved beam emittance.

ACKNOWLEDGEMENT

The authors acknowledge R.A. Bosch for providing his script for the B-model; C.-Y. Tsai for providing scripts for the analysis of MBI with Elegant; E. Allaria and E. Roussel for discussions on the MBI modeling and its impact on the FEL spectrum; W. M. Fawley and M. Cornacchia for helpful comments.

REFERENCES

[1] W. Decking and F. Obier, in *Proc. the 11th Europ. Part. Accel. Conf.*, Layout of the Beam Switchyard at the European XFEL, WEPC073, Genoa, Italy (2008).

[2] N. Milas and C. Gough, in *Proc. the 32nd Intern. Free Electron Laser Conf.*, Design of the SwissFEL Switchyard, WEPB16, Malmö, Sweden (2010).

[3] M. Placidi, J.-Y. Jung, A. Ratti, C. Sun, "Compact spreader schemes", *Nucl. Instr. Meth. Phys. Research A*, vol. 768, pp. 14–19, 2014.

[4] B. Faatz *et al.*, "Simultaneous operation of two soft x-ray free-electron lasers driven by one linear accelerator", *New J. Phys.*, vol. 18, p. 062002, 2016.

[5] T. Hara *et al.*, "Pulse-by-pulse multi-beam-line operation for x-ray free-electron lasers", *Phys. Rev. Accel. Beams*, vol. 19, p. 020703, 2016.

[6] E. Allaria *et al.*, "Highly coherent and stable pulses from the FERMI seeded free-electron laser in the extreme ultraviolet", *Nat. Photonics*, vol. 6, pp. 699–704, 2012.

[7] E. Allaria *et al.*, "Two-stage seeded soft-X-ray free-electron laser", *Nat. Photonics*, vol. 7, pp. 913–918, 2013.

[8] S. Di Mitri and S. Spampinati, *Phys. Rev. Accel. Beams*, vol. 20, p. 120701, 2017.

[9] S. Di Mitri, "Machine design and electron beam controlof a single-pass linac for free electron laser: the FERMI@Elettra case study", Ph.D Thesis, ISBN 978-90-367-5176-6,2011.

[10] S. Di Mitri *et al.*, "Design and simulation challenges for FERMI@elettra", *Nucl. Instrum. Methods Phys. Res. A,* vol. 608, pp. 19–27, 2009.

[11] E. Roussel *et al.*, "Multicolor High-Gain Free-Electron Laser Driven by Seeded Microbunching Instability", *Phys. Rev. Lett.*, vol. 115, p. 214801, 2015.

[12] E.L. Saldin, E.A. Schneidmiller, M. Yurkov, "Longitudinal space charge-driven microbunching instability in the TESLA Test Facility linac", *Nucl. Instrum. Methods Phys. Res. A*, vol. 528, p. 355.

[13] S. Spampinati *et al.*, "Laser heater commissioning at an externally seeded free-electron laser", *Phys. Rev. Special Topics – Accel. Beams*, vol. 17, p. 120705, 2014.

[14] S. Spaminati *et al.*, Commissioning of the FERMI@Elettra Laser Heater, in *Proc. the 34th Intern. Fre Electron Laser Conf.*, MOPD58, Nara Japan (2012).

[15] E. Allaria *et al.*, The FERMI free-electron lasers, J. Synchrotron Rad. 22 (2015) 485–491.

[16] Z. Huang and K.-J- Kim, "Formulas for coherent synchrotron radiation microbunching in a bunch compressor chicane", *Phys. Rev. Special Topics – Accel. Beams*, vol. 5, p. 074401 (2002).

[17] R.A. Bosch, K.J. Kleman and J. Wu, "Modeling two-stage bunch compression with wakefields: macroscopic properties and microbunching instability", *Phys. Rev. Special Topics – Accel. Beams*, vol. 11, p. 090702 (2008).

[18] D. Ratner, C. Behrens, Y. Ding, Z. Huang, A. Marinelli, T. Maxwell, and F. Zhou, "Time-resolved imaging of the microbunching instability and energy spread at the Linac Coherent Light Source", *Phys. Rev. Special Topics – Accel. Beams*, vol. 18, p. 030704 (2015).

[19] J. Qiang, R. D. Ryne, M. Venturini, A. A. Zholents, and I. V. Pogorelov, "High resolution simulation of beam dynamics in electron linacs for x-ray free electron lasers", *Phys.*

ISBN: 978-3-95450-206-6 doi:10.18429/JACoW-FLS2018-WEP2PT008

Rev. Special Topics – Accel. Beams, vol. 12, 100702 (2009).

[20] M. Venturini, "Models of longitudinal space-charge impedance for microbunching instability", *Phys. Rev. Special Topics – Accel. Beams*, vol. 11, p. 034401 (2008).

[21] Z. Huang *et al*., "Measurements of the linac coherent light source laser heater and its impact on the x-ray free-electron laser performance", *Phys. Rev. Special Topics – Accel. Beams*, vol. 13, p. 020703 (2010).

[22] S. Di Mitri, M. Cornacchia, S. Spampinati, "Cancellation of Coherent Synchrotron Radiation Kicks with Optics Balance", *Phys. Rev. Lett.*, vol. 110, p. 014801,2013.

[23] D. Ratner *et al*., "Experimental Demonstration of a Soft X-Ray Self-Seeded Free-Electron Laser", *Phys. Rev. Lett.* vol. 114, p. 054801 (2015).

[24] Z. Zhang, R. Lindberg, W. M. Fawley, Z. Huang, J. Krzywinski, A. Lutman, G. Marcus, and A. Marinelli, *Phys. Rev. Accel. Beams*, vol. 19, p. 050701 (2016).

[25] M. Venturini and A. Zholents, Modeling microbunching from shot noise using Vlasov solvers, *Nucl. Instr. Meth. Phys. Research A*, vol. 593, pp. 53–56, 2008.

[26] R. Bosch, K.J. Kleman and J. Wu, in *Proc. 23rd Part. Accel. Conf*., WE5RFP057, Vancouver, BC, Canada (2009).

[27] Ya.S. Derbenev, J. Rossbach, E.L. Saldin and V.D. Shiltsev, Microbunch radiative head-tail interaction, in *Proc. TESLA-FEL'95*, DESY, Hamburg, Germany (1995).

[28] C.-Y. Tsai, S. Di Mitri, D. Douglas, R. Li, and C. Tennant, "Conditions for coherent-synchrotron-radiation-induced microbunching suppression in multibend beam transport or recirculation arcs", *Phys. Rev. Accel. Beams*, vol. 20, 024401 (2017).

[29] M. G. Minty and F. Zimmermann, Beam Techniques – Beam Control and Manipulation, SLAC-R-621 (2003) and in *Proc. Lectures given at the US Particle Accelerator School*, University of Chicago and Argonne National Laboratory (1999).